A comprehensive approach to double inverted pendulum modelling

KAMIL ANDRZEJEWSKI, MATEUSZ CZYŻNIEWSKI, MACIEJ ZIELONKA,

RAFAŁ ŁANGOWSKI and TOMASZ ZUBOWICZ

The problem of mathematical modelling and indication of properties of a DIP has been investigated in this paper. The aim of this work is to aggregate the knowledge on a DIP modelling using the Euler-Lagrange formalism in the presence of external forces and friction. To indicate the main properties important for simulation, model parameters identification and control system synthesis, analytical and numerical tools have been used. The investigated properties include stability of equilibrium points, a chaos of dynamics and non-minimum phase behaviour around an upper position. The presented results refer to the model of a physical (constructed) DIP system.

Key words: double inverted pendulum, modelling, non-linear dynamics, Lagrangian mechanics

1. Introduction

A pendulum is one of the elementary physical systems which greatly impacts researchers and allows for understanding of the behaviour and properties of the surrounding world, e.g., the rotational movement of the Earth and the gravity. This also applies to the 'world of engineering' where solving a problem of an inverted pendulum control is one of the fundamental issues in automatics and robotics. This is evidenced by a large number of publications and available solutions. One of the most common applications using the stabilisation mechanism of an inverted pendulum are balancing robots, e.g., [1, 6, 9, 25], balancing vehicles,

e.g., [15, 16, 19, 24] and humanoid robots, e.g., [4, 13, 18]. Moreover, a pendulum allows studying the problem of synchronisation [17]. It is worth adding that the algorithms able to tackle the problem of oscillators synchronisation are considered important in the field of electrical power engineering, e.g., [5]. Hence, deriving a mathematical model of an inverted pendulum is of high significance from the practical point of view. It is because a cognitive model allows to, e.g., predict the behaviour of considered system or it can be used to derive the other models such as models for control and estimation purposes. Moreover, it is possible to extend an inverted pendulum to a structure of DIP. A typical DIP is primarily composed of two joined arms mounted either on a cart or rotating spindle. This concept allows to study i.a. structures and algorithms for control and (state) estimation for dynamic systems with higher-order non-linearity, e.g., [22].

Against the above background, the DIP may be considered as an under-actuated (more degrees of freedom than the number of control inputs) non-linear system with a high level of non-linearities [26]. Moreover, it is well-known that such systems hold more than one equilibrium point. There are four (physical) equilibrium points among which the only one stable (a bottom position) is in the case of the DIP. Additionally, for the same values of parameters and initial conditions as well as for their minor perturbations, the behaviour of the DIP may become unpredictable. It is a typical property of systems with chaotic dynamics [12, 20]. Hence, a deep understanding of the DIP properties has crucial meaning for design and control purposes for the above mentioned exemplary applications. As has been mentioned above, one of the widespread ways to analyse the behaviour and properties of systems is through studying their mathematical models. Three main approaches to modelling dynamics of the DIP can be distinguished. They rely on model derivation via Newton's laws of motion, Euler-Lagrange equation or Kane's method [3]. The first methodology is based on a balance of forces (torques) and it is very useful for implementation of control algorithms. This approach can be found, e.g., in [7, 21, 23–25]. The second method is the energy-based approach which allows i.a. the study of dynamic properties and it was shown, e.g., in [8, 26]. It is worth adding that both the impact of uncontrolled external forces and the effects of friction between the DIP construction elements are not considered in [26]. In turn, the DIP model in implicit ODE format is delivered and implemented in the Matlab environment in [8]. Also, this model has not taken into account the impact of uncontrolled external forces. An alternative approach is Kane's method which was used, e.g., in [11, 14].

The aim of this work is related to the problem of the DIP on a cart modelling. The presented derivation of the DIP cognitive model is based on the Euler-Lagrange formalism. The procedure includes the impact of external forces and the effects of friction between the DIP construction elements. The former is handled by introducing a concept of the generalised forces, while the latter

is handled by invoking Rayleigh dissipation function. This approach is usually considered more effective as the description of the energetic balance of the mechanical system is less tedious than utilising the Newtonian mechanics at least at the initial modelling step. The resulting model of the DIP is obtained in a specific case of DAE format. Under certain conditions, the DAE DIP model can be transformed into ODE format. This is an important step in model formulation. The numerical tools which are to be applied to handle the DAE or ODE problem have considerably different requirements, in general, and in particular, e.g., when a closed-loop control is applied. Typically, the DAE problem is numerically or algorithmically more demanding. Therefore, the chosen representation format determines the required set of numerical tools. In this paper, the ODE DIP model representation has been selected for numerical studies of the DIP. This is due to the fact that the ODE problem is numerically or algorithmically less demanding. The investigated properties include stability of equilibria, the chaos of the DIP dynamics and non-minimum phase behaviour around the upper position. In other words, the resulting model is used for prediction of the DIP behaviour. It should be added that this paper is based on results obtained in BSc thesis [2].

The paper is organised as follows. The problem formulation and main assumptions are presented in section 2. Next, the derivation of the DIP mathematical model is given in section 3. The properties of the DIP such as stability of equilibria, the chaos of the dynamics and non-minimum phase behaviour around an upper position are investigated in section 4. The paper is concluded in section 5.

2. Problem formulation

Taking $\mathbb{R}^n$ to denote a vector space over a field of real numbers $\mathbb{R}$ and in particular a co-domain of real-valued vector functions such as: $\mathbb{T} \rightarrow \mathbb{R}^n$, where $\mathbb{T}$ is an open set in $\mathbb{R}$, with usual addition and scalar multiplication satisfies an appropriate set of axioms and given symbolically by $+$ and $\cdot$, respectively and $\times$ as a Cartesian product. Moreover, consider $\mathbb{Z}_+$ to denote a positive part of an integer field and a set $\left(n_q, n_u, n_d\right) \subset \mathbb{Z}_+$. Then a cognitive mathematical model $\mathcal{M}_{\text{DIP}}$ of a physical DIP is understood as:

$$\mathcal{M}_{\text{DIP}} : \mathbb{X} \rightarrow \mathbb{R}^{n_q}, \tag{1}$$

where $\mathbb{X} \overset{\text{def}}{=} \mathbb{X}_q \times \mathbb{X}_u \times \mathbb{X}_d \subset \mathbb{R}^{n_q} \times \mathbb{R}^{n_u} \times \mathbb{R}^{n_d}$ denotes a region in the state, control and disturbance input spaces combined, respectively. Moreover, for clarity of presentation, one must consider $(X, Y, Z) \equiv \mathbb{R}^3$ to span a three dimensional Euclidean space in which the DIP operates.

The goal of this work is to deliver a comprehensive approach to the derivation and study of the properties of $\mathcal{M}_{\text{DIP}}$ in terms of its: phase portraits, stability, the chaos of dynamics and non-minimum phase behaviour around an upper position. For this purpose the following assumptions are formulated.

Assumption 1 *The pendulum is composed of interconnected rigid body elements.*

It causes that the geometry of the DIP elements does not distort during operation under considered load.

Assumption 2 *Movement is considered in two dimensions.*

The movement is constrained to the (X, Y) plane by the DIP geometry which disallows the rotation around the X and Y axes.

Assumption 3 *Linear motion in the X axis is not constrained.*

For analysing the cognitive model of the DIP the linear motion of a cart is unconstrained by gantry length.

Assumption 4 *Friction effects are modelled by Rayleigh dissipation function.*

By assumption, the model of friction includes only viscosity phenomena. Since the DIP joints contain bearings the other components of friction can be neglected.

Assumption 5 *The $\mathcal{M}_{\text{DIP}}$ structure and parameters are considered to be perfectly known.*

Assumption 6 *The disturbance inputs (the uncontrolled external forces) are considered to be external forces and torques applied to the DIP components.*

3. Cognitive model of DIP

The DIP is taken under consideration as depicted in Fig. 1. It is composed of five main elements. First, the 'cart' constitutes the basis of the DIP. It is mounted on the second element, namely the 'gantry'. The connection restricts the movement of the 'cart' only to one degree of freedom which is the linear movement in X direction (with respect to assumption 3). The third element is the 'first arm' which is mounted on the 'cart' at a mounting point called 'first joint'. Analogously, the 'second arm' (the fourth element) is connected to the 'first arm' via the 'second joint'. Both considered joints comprise a bearing and

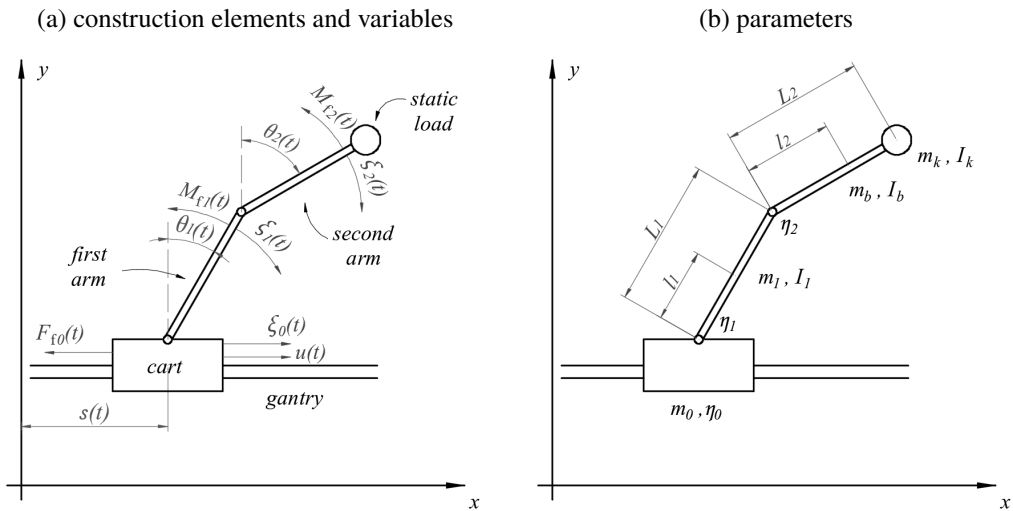(a) construction elements and variables   (b) parameters

Figure 1: Graph of the DIP.

are restricted to only allow rotary motion with respect to the Z axis and by such restrict the movement of the arms to (X, Y) plane (which justifies assumption 2). The fifth element is the 'static load' mounted on the unlinked end of the 'second arm'.

Movement of the cart is characterised by linear displacement $s(t)$ and velocity $\dot{s}(t)$. The rotary motion of the arms, by analogy, are characterised by angular displacement $\theta_i(t)$ and angular velocity $\dot{\theta}_i(t)$, $\forall i \in \overline{1, 2}$. In order to set the DIP in motion an external input force $u(t)$ is applied to the cart and $\forall t \in \mathbb{T} : u(t) \in \mathbb{X}_\mathrm{u}$. Moreover, by assumption 6 the surrounding environment can exerts additional impact on the DIP through additional (uncontrolled) external force $\xi_0(t)$ and torques $\xi_i(t)$, $\forall i \in \overline{1, 2}$, acting on the cart and arms, respectively. Additionally, according to assumption 4 the viscous friction between the cart and the gantry and within the joints is marked by $F_{\mathrm{f}0}(t)$, $M_{\mathrm{f}1}(t)$ and $M_{\mathrm{f}2}(t)$, respectively. Utilising this characterisation allows one to define the overall DIP position, velocity and disturbance inputs vectors as:

$$\boldsymbol{q}(t) \stackrel{\text{def}}{=} [s(t), \theta_1(t), \theta_2(t)]^T, \qquad \dot{\boldsymbol{q}}(t) \stackrel{\text{def}}{=} \left[\dot{s}(t), \dot{\theta}_1(t), \dot{\theta}_2(t)\right]^T,$$

$$\boldsymbol{\xi}(t) \stackrel{\text{def}}{=} [\xi_0(t), \xi_1(t), \xi_2(t)]^T,$$

respectively, and clearly $\dot{\boldsymbol{q}}(t) \equiv \dfrac{\mathrm{d}}{\mathrm{d}t}\boldsymbol{q}(t)$ and $\forall t \in \mathbb{T} : [\dot{\boldsymbol{q}}(t)^T, \boldsymbol{q}(t)^T]^T \in \mathbb{X}_\mathrm{q}$, $\boldsymbol{\xi}(t) \in \mathbb{X}_\mathrm{d}$.

The main parameters of the DIP are marked in Fig. 1b. These are: m_0, m_1, m_b, m_k – masses of: the cart, first arm, second arm and static load, respectively;

L_i – the length of arm, $\forall i \in \overline{1, 2}$; η_0, η_1, η_2 – friction coefficients between the cart and the gantry and within the joints, respectively. In turn, l_i denotes the distance from the beginning of the arm to its centre of gravity, $\forall i \in \overline{1, 2}$ and I_1, I_b and I_k are the moments of inertia for first arm, second arm and static load, respectively. Moreover, m_2 and I_2 stand for the equivalents mass and moment of inertia including the second arm and the static load, respectively. The values of parameters have been given in Appendix A.

Following Hamilton's principal and using the tools of the calculus of variation the second order partial differential equation of Euler–Lagrange type is obtained. However, in order to include the external forces and friction a modification to the Euler–Lagrange equation is required which yields:

$$\frac{\mathrm{d}}{\mathrm{d}t} \left(\frac{\partial L(\dot{\boldsymbol{q}}(t), \boldsymbol{q}(t))}{\partial \dot{\boldsymbol{q}}(t)} \right) - \frac{\partial L(\dot{\boldsymbol{q}}(t), \boldsymbol{q}(t))}{\partial \boldsymbol{q}(t)} + \frac{\partial D(\dot{\boldsymbol{q}}(t))}{\partial \dot{\boldsymbol{q}}(t)} = \boldsymbol{Q}(u(t), \boldsymbol{\xi}(t)), \quad (2)$$

where: L denotes the Lagrangian, D is the Rayleigh dissipation function and $\boldsymbol{Q}$ is a vector of external forces and torques.

The first two terms on the left-hand side of (2) are to model the effects of the conservative forces. The third element on the left-hand side and the element on the right-hand side are to account for the non-conservative effects of friction and the external forces, respectively.

The Lagrangian is defined as a difference between the total kinetic (E_k) and potential (E_p) energies according to:

$$L(\dot{\boldsymbol{q}}(t), \boldsymbol{q}(t)) \stackrel{\text{def}}{=} E_k(\dot{\boldsymbol{q}}(t)) - E_p(\boldsymbol{q}(t)). \quad (3)$$

Both the total kinetic and potential energies are given by the sum of the energies related to each of the components of the DIP: the cart, first and second arm (including the static load), respectively. Therefore:

$$E_k(\dot{\boldsymbol{q}}(t)) = \sum_{i \in \overline{0,2}} E_{k\,i}(\dot{\boldsymbol{q}}(t)), \quad (4)$$

where:

$$E_{k\,0}(\dot{\boldsymbol{q}}(t)) = \frac{1}{2} m_0 \dot{s}(t)^2, \quad (5a)$$

$$E_{k\,1}(\dot{\boldsymbol{q}}(t)) = \frac{1}{2} m_1 \dot{s}(t)^2 + m_1 \dot{s}(t) \dot{\theta}_1(t) l_1 \cos \theta_1(t)$$
$$+ \frac{1}{2} m_1 \dot{\theta}_1(t)^2 l_1^2 + \frac{1}{2} I_1 \dot{\theta}_1(t)^2, \quad (5b)$$

$$E_{k2}(\dot{\boldsymbol{q}}(t)) = \frac{1}{2}m_2\dot{s}(t)^2 + \frac{1}{2}m_2\dot{\theta}_1(t)^2L_1^2 + \frac{1}{2}m_2\dot{\theta}_2(t)^2l_2^2$$
$$+ m_2\dot{s}(t)\dot{\theta}_1(t)L_1\cos\theta_1(t) + m_2\dot{s}(t)\dot{\theta}_2(t)l_2\cos\theta_2(t)$$
$$+ m_2\dot{\theta}_1(t)L_1\dot{\theta}_2(t)l_2\cos(\theta_1(t)-\theta_2(t)) + \frac{1}{2}I_2\dot{\theta}_2(t)^2, \quad (5c)$$

and:

$$E_p(\boldsymbol{q}(t)) = \sum_{i\in 0,2} E_{pi}(\boldsymbol{q}(t)), \quad (6)$$

where:

$$E_{p0}(\boldsymbol{q}(t)) = 0, \quad (7a)$$

$$E_{p1}(\boldsymbol{q}(t)) = l_1m_1g\cos\theta_1(t), \quad (7b)$$

$$E_{p2}(\boldsymbol{q}(t)) = m_2gL_1\cos\theta_1(t) + m_2gl_2\cos\theta_2(t). \quad (7c)$$

Following assumption 4 and selecting a quadratic form for Rayleigh dissipation function to account for the friction energy loss yields:

$$D(\dot{\boldsymbol{q}}(t)) \overset{\text{def}}{=} \frac{1}{2}\dot{\boldsymbol{q}}^T(t)\boldsymbol{\eta}\dot{\boldsymbol{q}}(t). \quad (8)$$

Including the viscous friction (see Fig. 1a) between the cart and the gantry and within the joints as:

$$F_{f0}(t) = \eta_0\dot{s}(t), \quad (9a)$$
$$M_{f1}(t) = \eta_1\dot{\theta}_1(t) + \eta_2\dot{\theta}_1(t) - \eta_2\dot{\theta}_2(t), \quad (9b)$$
$$M_{f2}(t) = \eta_2\dot{\theta}_2(t) - \eta_2\dot{\theta}_1(t), \quad (9c)$$

yields the support of (8):

$$\boldsymbol{\eta} = \begin{bmatrix} \eta_0 & 0 & 0 \\ 0 & \eta_1+\eta_2 & -\eta_2 \\ 0 & -\eta_2 & \eta_2 \end{bmatrix}. \quad (10)$$

The external forces are defined as:

$$\boldsymbol{Q}(u(t),\boldsymbol{\xi}(t)) \overset{\text{def}}{=} \left[Q_0(u(t),\boldsymbol{\xi}(t)),\ Q_1(u(t),\boldsymbol{\xi}(t)),\ Q_2(u(t),\boldsymbol{\xi}(t))\right]^T \quad (11)$$

with individual components given by

$$(Q_0,Q_1,Q_2)(u(t),\boldsymbol{\xi}(t)) = (u(t)+\xi_0(t),\xi_1(t),\xi_2(t)).$$

Inserting (3), (8) and (11) into (2) and performing the necessary calculations yields $\mathcal{M}_{\text{DIP}}$ in the DAE format given by:

$$\mathcal{M}_{\text{DIP}}^{\text{DAE}}: \quad \boldsymbol{H}(\boldsymbol{q}(t))\ddot{\boldsymbol{q}}(t) + \boldsymbol{C}(\dot{\boldsymbol{q}}(t), \boldsymbol{q}(t))\dot{\boldsymbol{q}}(t) + \boldsymbol{g}(\boldsymbol{q}(t)) = \boldsymbol{Q}(u(t), \boldsymbol{\xi}(t)), \quad (12)$$

where: $\ddot{\boldsymbol{q}}(t) \equiv \dfrac{\mathrm{d}}{\mathrm{d}t}\dot{\boldsymbol{q}}(t)$,

$$\boldsymbol{H}(\boldsymbol{q}(t)) = \begin{bmatrix} m_0+m_1+m_2 & (m_1l_1+m_2L_1)\cos\theta_1(t) & m_2l_2\cos\theta_2(t) \\ (m_1l_1+m_2L_1)\cos\theta_1(t) & m_1l_1^2+m_2L_1^2+I_1 & m_2L_1l_2\cos(\theta_1(t)-\theta_2(t)) \\ m_2l_2\cos\theta_2(t) & m_2L_1l_2\cos(\theta_1(t)-\theta_2(t)) & m_2l_2^2+I_2 \end{bmatrix}, \quad (13a)$$

$$\boldsymbol{C}(\dot{\boldsymbol{q}}(t), \boldsymbol{q}(t)) = \begin{bmatrix} \eta_0 & -(m_1l_1+m_2L_1)\sin\theta_1(t)\dot{\theta}_1(t) & -m_2l_2\sin\theta_2(t)\dot{\theta}_2(t) \\ 0 & \eta_1+\eta_2 & m_2L_1l_2\sin(\theta_1(t)-\theta_2(t))\dot{\theta}_2(t)-\eta_2 \\ 0 & m_2L_1l_2\sin(\theta_1(t)-\theta_2(t))\dot{\theta}_1(t)-\eta_2 & \eta_2 \end{bmatrix}, \quad (13b)$$

$$\boldsymbol{g}(\boldsymbol{q}(t)) = \begin{bmatrix} 0 \\ -(m_1l_1+m_2L_1)\,g\sin\theta_1(t) \\ -m_2l_2g\sin\theta_2(t) \end{bmatrix}. \quad (13c)$$

It should be noticed that $\boldsymbol{H}(\boldsymbol{q}(t))$ can be interpreted as the system inertia. Therefore, the physical properties of the system imply that the inverse of $\boldsymbol{H}(\boldsymbol{q}(t))$ exists [20]. Unfortunately, in the $\mathcal{M}_{\text{DIP}}$ case, the structure of $\boldsymbol{H}(\boldsymbol{q}(t))$ causes that demonstrating its positive definiteness is not obvious. Therefore, alternative ways such as using appropriate assessments or numerical approach may be used. The former though successfully utilised in [26] is not applicable in the considered case. Therefore, the latter approach has been presented in this paper. In particular, firstly (12) can be rewritten as:

$$\mathcal{M}_{\text{DIP}}^{\text{DAE}}: \quad \boldsymbol{H}(\boldsymbol{q}(t))\ddot{\boldsymbol{q}}(t) = \boldsymbol{B}(\dot{\boldsymbol{q}}(t), \boldsymbol{q}(t), u(t), \boldsymbol{\xi}(t)), \quad (14)$$

where $\boldsymbol{B}(\dot{\boldsymbol{q}}(t), \boldsymbol{q}(t), u(t), \boldsymbol{\xi}(t)) = \boldsymbol{Q}(u(t), \boldsymbol{\xi}(t)) - \boldsymbol{C}(\dot{\boldsymbol{q}}(t), \boldsymbol{q}(t))\dot{\boldsymbol{q}}(t) - \boldsymbol{g}(\boldsymbol{q}(t))$.

In order to obtain ODE formulation (14) it is necessary to prove that $\boldsymbol{H}(\boldsymbol{q}(t))^{-1}$ exists. It is obvious that:

$$\boldsymbol{H}(\boldsymbol{q}(t))^{-1} = \frac{1}{\det(\boldsymbol{H}(\boldsymbol{q}(t)))}\,(\boldsymbol{H}(\boldsymbol{q}(t))_{\text{ad}})^T, \quad (15)$$

where $\boldsymbol{H}(\boldsymbol{q}(t))_{\text{ad}}$ stands for the adjunct matrix of $\boldsymbol{H}(\boldsymbol{q}(t))$.

Hence, $\boldsymbol{H}(\boldsymbol{q}(t))$ has to be non-singular, therefore:

$$\det(\boldsymbol{H}(\boldsymbol{q}(t)) \neq 0. \quad (16)$$

It is easy to notice that the determinant of $\boldsymbol{H}(\boldsymbol{q}(t))$ is also the denominator $(M(\theta_1(t), \theta_2(t)))$ of (15). Therefore, the sign of $M(\theta_1(t), \theta_2(t))$ will be checked in

the further part of this section by simulation. The polynomial of the denominator is as follows:

$$
\begin{aligned}
M(\theta_1(t), \theta_2(t)) = {} & h_{11}h_{22}h_{33} \\
& + 2h_{12}h_{13}h_{23} \cos \theta_1(t) \cos \theta_2(t) \cos(\theta_1(t) - \theta_2(t)) \\
& - h_{33}h_{12}^2 \cos^2 \theta_1(t) - h_{11}h_{23}^2 \cos^2(\theta_1(t) - \theta_2(t)) \\
& - h_{22}h_{13}^2 \cos^2 \theta_2(t),
\end{aligned}
\tag{17}
$$

where:

$$h_{11} = m_0 + m_1 + m_2, \tag{18a}$$

$$h_{12} = h_{21} = m_1 l_1 + m_2 L_1, \tag{18b}$$

$$h_{13} = h_{31} = m_2 l_2, \tag{18c}$$

$$h_{22} = m_1 l_1^2 + m_2 L_1^2 + I_1, \tag{18d}$$

$$h_{23} = h_{32} = m_2 L_1 l_2, \tag{18e}$$

$$h_{33} = m_2 l_2^2 + I_2. \tag{18f}$$

Let $\theta_1(t), \theta_2(t) \in (-\pi, \pi]$ [rad] and the arbitrary set of parameters which has been shown in Table 1 (see Appendix A). The graph of the denominator's value is illustrated in Fig. 2. As can be noticed in Fig. 2 the value of $M(\theta_1(t), \theta_2(t))$ does not reach zero. Hence, this implies the non-singularity of the matrix $\boldsymbol{H}(\boldsymbol{q}(t))$, what should have been proved.
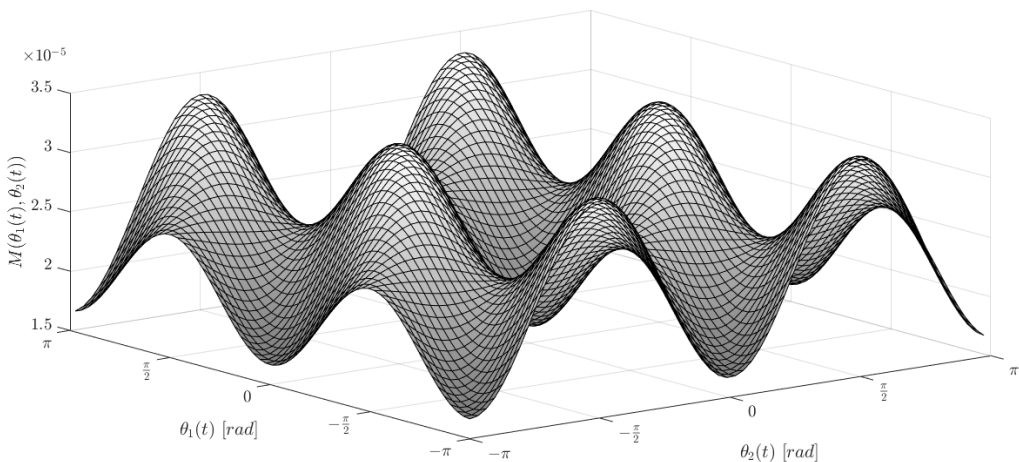

Figure 2: The graph of denominator's value.

Moreover, assuming the natural behaviour of internal dynamics of the DIP, i.e.,:

- taking into account the friction effects, for every initial conditions excluding the upper equilibrium point (the upper position), the DIP will lose kinetic energy, slowing down and going to the bottom equilibrium point (the bottom position), and

- including that the bottom equilibrium point is asymptotically stable,

it is possible to show the convergence of the $M(\theta_1(t), \theta_2(t))$ to a finite value.

Taking (17) at P_4 (see section 4.1) with $s = 0$ yields:

$$M(\theta_1(t), \theta_2(t)) \approx 1,6691 \times 10^{-5}. \tag{19}$$

The above result has been illustrated in Fig. 3 for a chosen set of points – initial conditions. These points were selected arbitrarily from a neighbourhood of an upper (equilibrium) position while excluding the equilibrium point itself. It allows the investigation of the impact of a wide range of change of instantaneous values of state variables on the denominator values.
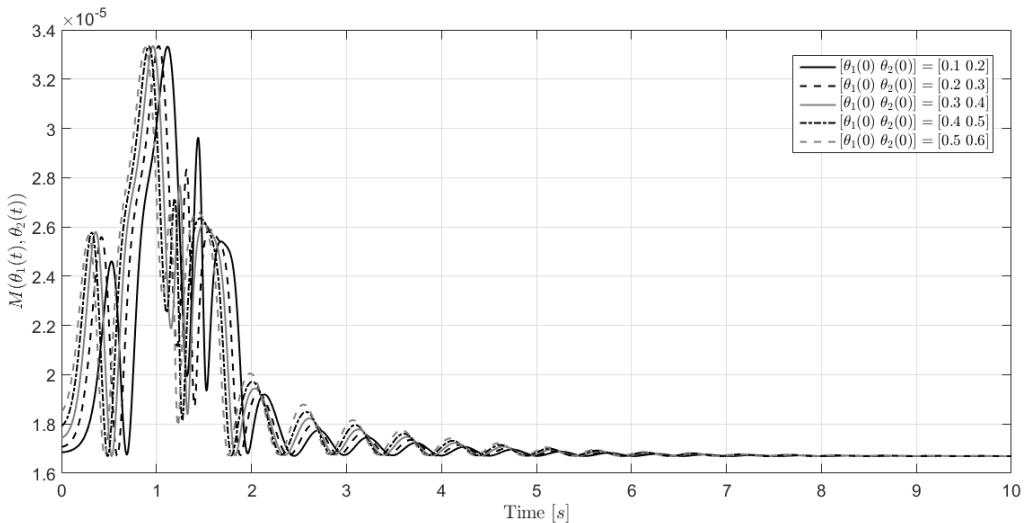
Figure 3: The value of denominator for different initial conditions.

Using this fact allows one to rewrite the DAE DIP model in equivalent ODE format as:

$$\mathcal{M}_{\text{DIP}}^{\text{ODE}} : \quad \ddot{\boldsymbol{q}}(t) + \widetilde{\boldsymbol{C}}(\dot{\boldsymbol{q}}(t), \boldsymbol{q}(t))\dot{\boldsymbol{q}}(t) + \widetilde{\boldsymbol{g}}(\boldsymbol{q}(t)) = \widetilde{\boldsymbol{Q}}(\boldsymbol{q}(t), u(t), \boldsymbol{\xi}(t)), \tag{20}$$

where:

$$\widetilde{C}(\dot{q}(t), q(t)) = H(q(t))^{-1} C(\dot{q}(t), q(t)), \tag{21a}$$

$$\widetilde{g}(q(t)) = H(q(t))^{-1} g(q(t)), \tag{21b}$$

$$\widetilde{Q}(q(t), u(t), \xi(t)) = H(q(t))^{-1} Q(u(t), \xi(t)). \tag{21c}$$

Following principal properties of explicit ODE formulation the $\mathcal{M}_{\text{DIP}}^{\text{ODE}}$ can be rewritten in state space format as $\mathcal{M}_{\text{DIP}}^{\text{SS}}$.

As it was mentioned above, in this paper the ODE DIP model representation has been selected for numerical studies of the DIP properties. Hence, in the further parts of this manuscript the $\mathcal{M}_{\text{DIP}}$ refers to $\mathcal{M}_{\text{DIP}}^{\text{ODE}}$.

4. Properties of DIP

In this section, certain properties of the DIP are investigated and analysed using the Matlab/Simulink environment. As it has been mentioned in the previous section, the $\mathcal{M}_{\text{DIP}}$ in ODE format will be further considered. Thus, (20) has been implemented in the Matlab/Simulink environment and the proper numerical procedures have been utilised. This model has been used to study the DIP behaviour as well as the stability of equilibria and chaos of the DIP dynamics by using phase portraits. In turn, in order to study the stability based on Lyapunov theory and demonstrate the non-minimum phase behaviour around the upper position of the DIP, the necessity of deriving linear model has appeared. Therefore, the Taylor series expansion (neglecting the second and higher-order terms) has been used to obtain the linear approximation of (20). This approximation can be written as follows:

$$\begin{aligned}
\nabla_{\ddot{q}(t)} F \big|_{\text{P}} (\ddot{q}(t) - \ddot{q}_{\text{e}}) &= \nabla_{[\dot{q}(t)^T, q(t)^T]^T}^T F \big|_{\text{P}} \left(\left[\dot{q}(t)^T, q(t)^T \right]^T - \left[\dot{q}_{\text{e}}^T, q_{\text{e}}^T \right]^T \right) \\
&+ \nabla_{u(t)} F \big|_{\text{P}} (u(t) - u_{\text{e}}) + \nabla_{\xi(t)} F \big|_{\text{P}} (\xi(t) - \xi_{\text{e}}),
\end{aligned} \tag{22}$$

where: $F \overset{\text{def}}{=} F\left(\ddot{q}(t), \dot{q}(t), q(t), u(t), \xi(t)\right)$ is (20) in its general form, $\nabla_{(\cdot)}$ denotes a gradient in the direction of $(\cdot)$ and $\text{P} \overset{\text{def}}{=} (\ddot{q}_{\text{e}}, \dot{q}_{\text{e}}, q_{\text{e}}, u_{\text{e}}, \xi_{\text{e}}) \in \mathbb{R}^{n_q} \times \mathbb{X}_q \times \mathbb{X}_u \times \mathbb{X}_d$ stands for an equilibrium point of F.

Since this section involves simulation experiments, let $\mathbb{R} \times \mathbb{R} \times \mathbb{R} \times \mathbb{R} \times (-\pi, \pi] \times (-\pi, \pi] \subset \mathbb{X}_q$, $[-u_{\max}, u_{\max}] \subset \mathbb{X}_u$ and $\forall t \in \mathbb{T} : \xi(t) \in \emptyset$, where: $u_{\max}$ is the maximum force that can be applied to the cart. An arbitrary set of the DIP parameter values and the maximum value of force have been given in Appendix A.

4.1.   Basic properties of DIP

A comprehensive description of the DIP behaviour results directly from $\boldsymbol{F}$. Therefore, analysing $\boldsymbol{F}$ in the considered domain allows one to characterise the basic properties of the DIP. One of the useful tools that can be used for the analysis of the DIP internal dynamics is the vector field (the field of directions). Due to 'high' dimensionality of the DIP this is done by illustrating the subspaces in terms of the planes: $(s, \dot{s})$, $(\theta_1, \dot{\theta}_1)$, and $(\theta_2, \dot{\theta}_2)$ (which correspond to the $\mathbb{X}_q$ subspaces and the construction elements of the DIP) as depicted in Fig. 4.

It is clear that arrows in Fig. 4 illustrate the directions in which the internal dynamics of $\boldsymbol{F}$ drives the state of the DIP. This allows one to predict the state trajectory realisation for a given experiment starting at an arbitrarily chosen point in the considered domain of the DIP.

Moreover, in Fig. 4 an additional set of points has been shown. These points represent the equilibrium points of $\boldsymbol{F}$ which are identified in the following way. Assuming the lack of influence of external forces and torques the equilibrium points of the DIP in the considered domain can be determined as follows:

$$\boldsymbol{F}\left(\ddot{\boldsymbol{q}}(t), \dot{\boldsymbol{q}}(t), \boldsymbol{q}(t), u(t), \boldsymbol{\xi}(t)\right)\big|_{[\ddot{\boldsymbol{q}}(t)^T, \dot{\boldsymbol{q}}(t)^T]=\boldsymbol{0}} = 0, \tag{23}$$

which yields $P_j = \left(\ddot{s}_e, \ddot{\theta}_{1e}, \ddot{\theta}_{2e}, \dot{s}_e, \dot{\theta}_{1e}, \dot{\theta}_{2e}, s_e, \theta_{1e}, \theta_{2e}, u_e, \xi_{0e}, \xi_{1e}, \xi_{2e}\right)$, $\forall j \in \overline{1,4}$. Clearly:

$$P_1 = (0, 0, 0, 0, 0, 0, s, 0, 0, 0, 0, 0, 0), \tag{24a}$$
$$P_2 = (0, 0, 0, 0, 0, 0, s, \pi, 0, 0, 0, 0, 0), \tag{24b}$$
$$P_3 = (0, 0, 0, 0, 0, 0, s, 0, \pi, 0, 0, 0, 0), \tag{24c}$$
$$P_4 = (0, 0, 0, 0, 0, 0, s, \pi, \pi, 0, 0, 0, 0), \tag{24d}$$

where: $s \in \mathbb{R}$ and P_1 and P_4 are the already mentioned upper and bottom position, respectively.

It should be noticed that all the equilibrium points are characterised by twelve fixed values and $s \in \mathbb{R}$. It represents the natural behaviour of the unforced DIP. Clearly, taking non-zero initial conditions the cart will be forced to move in response to the arms movement by the momentum conservation principle. The effects of friction will decelerate the movement and the cart will stop at certain position s. This is illustrated in Fig. 4a by a 'horizontal' line.
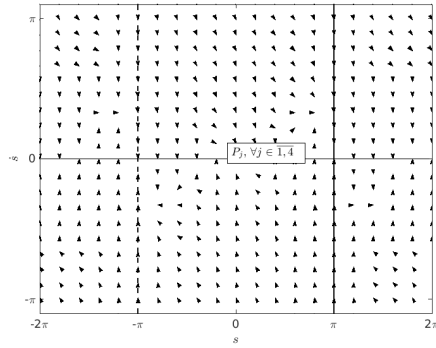
It is worth adding that both the vector field and the equilibrium points combined allow one to acquire basic knowledge on the attraction and repulsion of the equilibria and the related basins of attraction.
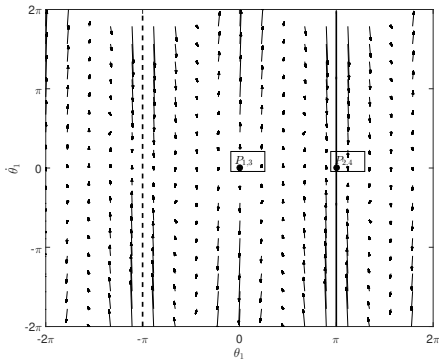
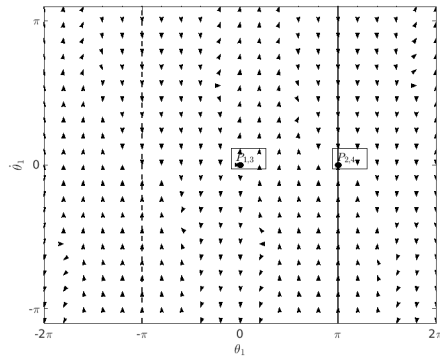(a) $(s, \dot{s})$ – plane (with information on derivative value)
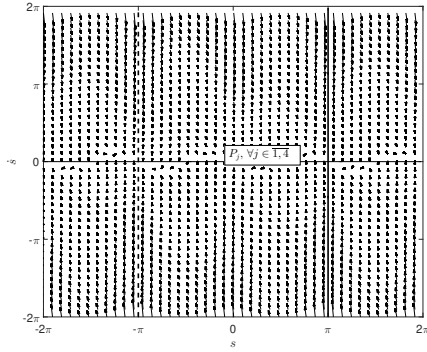
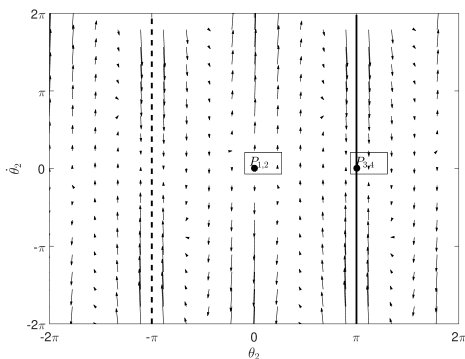(b) $(s, \dot{s})$ – plane (zoom including only directions)

(c) $(\theta_1, \dot{\theta}_1)$ – plane (with information on derivative value)

(d) $(\theta_1, \dot{\theta}_1)$ – plane (zoom including only directions)

(e) $(\theta_2, \dot{\theta}_2)$ – plane (with information on derivative value)

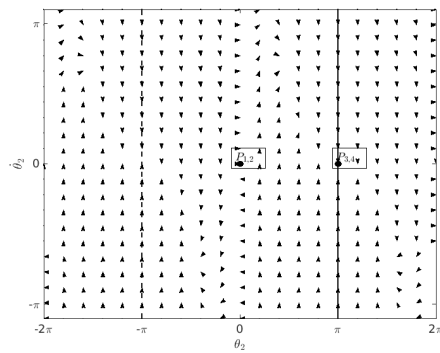(f) $(\theta_2, \dot{\theta}_2)$ – plane (zoom including only directions)

Figure 4: The DIP field of directions.

4.2. Stability

As already noticed by analysing Fig. 4 only one of the four equilibrium points attracts the state trajectories of the DIP, namely P_4 which corresponds to the bottom position of the DIP. Therefore, only P_4 under certain conditions can be identified as stable. The stability of P_4 is studied in the Lyapunov sense.

Definition 1 *[10] The equilibrium point $x = 0$ of $\dot{x} = f(x)$ is:*

- *stable if, for each $\epsilon > 0$, there is $\delta = \delta(\epsilon) > 0$ such that:*

$$\|x(0)\| < \delta \implies \|x(t)\| < \epsilon, \forall t \geqslant 0,$$

- *unstable if not stable,*

- *asymptotically stable if it is stable and δ can be chosen such that:*

$$\|x(0)\| < \delta \implies \lim_{t \to \infty} x(t) = 0.$$

Unfortunately, the direct application of this definition is impossible due to the above-mentioned feature of P_4. Clearly, P_4 is a hyperplane which acts as a state trajectory attractor as discussed in the previous section (see Fig. 4). However, it is possible to handle the stability of equilibria in terms of definition 1 by considering the DIP arms related subsystem (omitting the cart). This is done by invoking the following theorem.

Theorem 1 *[10] Let $x = 0$ be an equilibrium point for the non-linear system*

$$\dot{x} = f(x)$$

where $f : K \to \mathbb{R}^n$ is continuously differentiable and K is a neighbourhood of the origin. Let

$$A = \nabla_x f(x)|_{x=0}.$$

Then,
1. The origin is asymptotically stable if $Re \lambda_i < 0$ for all eigenvalues of A.
2. The origin is unstable if $Re \lambda_i > 0$ for one or more of the eigenvalues of A.

The matrix A, in considered case of the DIP, for the jth equilibrium point P_j, $\forall j \in \overline{1, 4}$ is as follows:

$$A_j = \nabla_{[\dot{\theta}_1(t), \dot{\theta}_2(t), \theta_1(t), \theta_2(t)]} F\Big|_{P_j}. \tag{25}$$

Hence, in order to study the stability of equilibria P_j the eigenvalues λ of appropriate A should be found. For the arbitrary set of parameters (see Appendix A) they are:

$$\lambda(A_1) \approx \begin{bmatrix} -17.06, & -6.52, & 7.47, & 5.73 \end{bmatrix}, \tag{26a}$$

$$\lambda(A_2) \approx \begin{bmatrix} 6.49, & -0.88+8.71j, & -0.88-8.71j, & -9.58 \end{bmatrix}, \tag{26b}$$

$$\lambda(A_3) \approx \begin{bmatrix} 7.93, & -9.72, & -1.53+7.71j, & -1.53-7.71j \end{bmatrix}, \tag{26c}$$

$$\lambda(A_4) \approx \begin{bmatrix} -4.86+9.93j, & -4.86-9.93j, & -0.32+6.24j, & -0.32-6.24j \end{bmatrix}. \tag{26d}$$

The above results confirm earlier observations that only the equilibrium point P_4 could be stable. In other words, because A_4 is Hurwitz, P_4 is locally asymptotically stable.

4.3. Chaos

Although the presented vector field allows one to assess i.a. the basin of attraction of the equilibrium point (P_4) one of the fundamental properties of the DIP remains elusive due to the limited resolution of this graphical description. This is manifested by the DIP high sensitivity to infinitesimal changes in the initial conditions, and it involves significant and even counter-intuitive distances between the state trajectories. This is one of the properties that identify a system as chaotic. This feature can be observed by using different tools such as a Lyapunov exponent and phase portraits. The Lyapunov exponent λ_L is a characteristic feature of a given system, determining its sensitivity to perturbations of the initial conditions, and is, therefore, one of the ways to determine the irregularity of motion of a system. If its value is greater than zero, then the initial distance between state trajectories $d(0)$, resulting from infinitesimal differences in initial conditions, will increase as the system evolves and the motion becomes chaotic. In order to investigate this property of the DIP the initial values problem involving $\mathcal{M}_{DIP}$ has been solved. Assuming $\mathbb{X}_0 \in \mathbb{X}$ in three independent simulation runs by perturbing the initial conditions $\mathbb{X}_0$, that is $\forall k \in \overline{1,3}$ as:

$$\begin{aligned} \dot{q}(0)^T &= k \cdot 10^{-4} \cdot \mathbf{1}^{3\times1}, \\ q(0)^T &= [0, 0, 0.1]^T + k \cdot 10^{-3} \cdot \mathbf{1}^{3\times1}, \end{aligned} \tag{27}$$

where $\mathbf{1}$ denotes a matrix with all elements equal 1, the distances between all combinations of the state trajectories sets have been calculated using:

$$\forall(\alpha,\beta) \in \{(1,2),(1,3)\}, \quad \forall t \in T_E: \quad d_{\alpha,\beta}(t) = \|x_\alpha(t) - x_\beta(t)\|_2, \tag{28}$$

where $x_{(\cdot)}(t)$ is a state trajectory starting at perturbed initial conditions in the subspace of state space (omitting the cart), T_E denotes simulation experiment period, and $\| \cdot \|_2$ stands for Euclidean norm.

The obtained trajectories of the distances between state trajectory have been illustrated in Fig. 5.
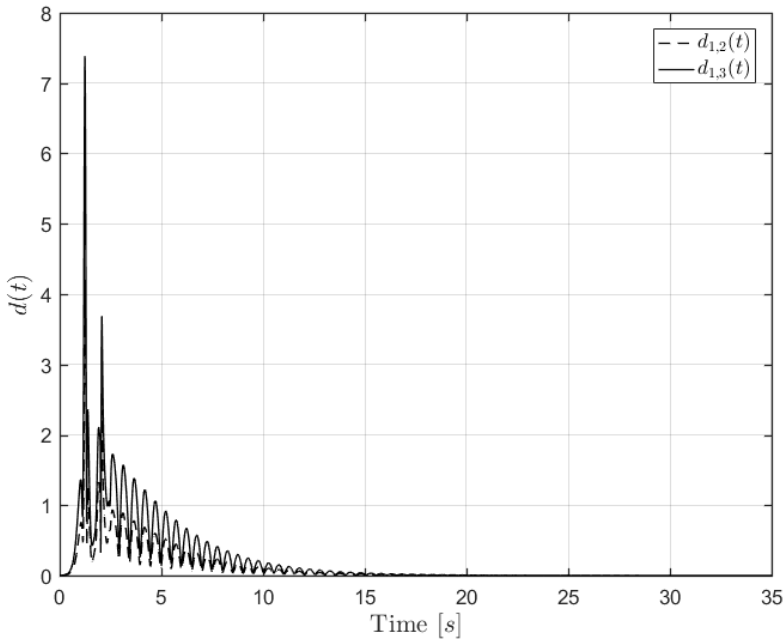

Figure 5: The trajectories of the distances between state trajectories.

The relation between $\lambda_L(t)$ and the state trajectory distances is given by:

$$\lambda_{L\,\alpha,\beta}(t) = \lim_{d_{\alpha,\beta}(0)\to 0} \frac{1}{t} \ln \frac{d_{\alpha,\beta}(t)}{d_{\alpha,\beta}(0)}. \tag{29}$$

In turn, the $\lambda_L(t)$ trajectories, $\forall t \in T_E$, have been presented in Fig. 6

As it can be noticed, the instantaneous values of Lyapunov's exponents change from positive to negative. This behaviour is expected for considered DIP. It is due to the fact that the DIP reaches only one stable equilibrium point P_4 (see section 4.2) where the real parts of Lyapunov exponents have negative values. Therefore, all state trajectories converge to this point, as illustrated by the distances between them converging to zero (see Fig. 5). However, the initially distances increase and represent the diverge of the trajectory from each other. It can be noticed in Fig. 7, where the trajectories starting from neighbouring initial conditions diverge over the transition considerable, e.g., Fig. 7b or even move in
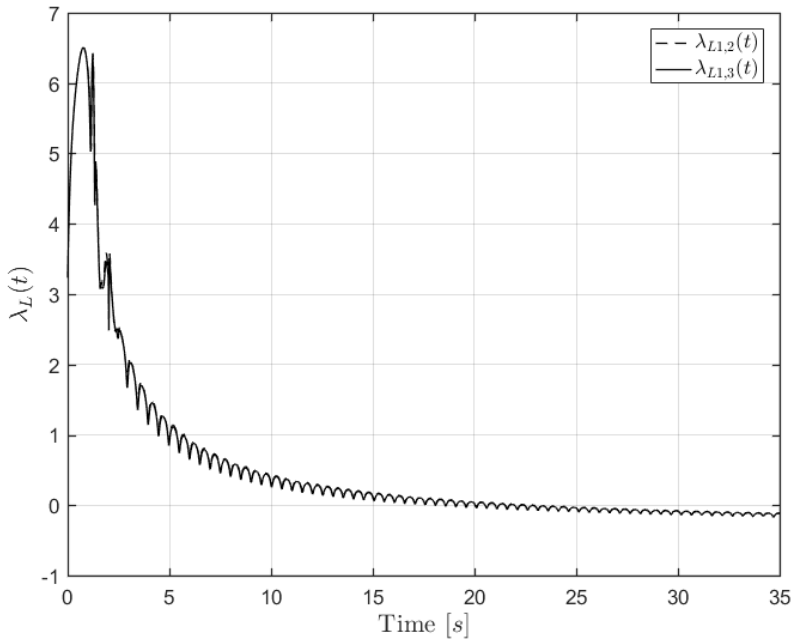
Figure 6: The Lyapunov exponents trajectories.

opposite directions, e.g., Fig. 7a [1]. It translates into positive instantaneous values of Lyapunov's exponents. Thus, it is clear that a slight perturbation of the initial conditions causes the stable point to be reached through completely different state trajectories. Hence, the above considerations confirm that the DIP is a chaotic system.

### 4.4.   Non-minimum phase behaviour around the upper position

As it has been mentioned in the introduction, the stabilisation mechanism of an inverted pendulum, especially in the upper position, is considered important for a large number of engineering applications. Therefore, it is very useful to acquire information on the DIP frequency domain characteristic. In this work, it is done for P_1 and its close neighbourhood in the following manner.

Taking a minimum realisation of $\left(A_1, B_1, \left[0^{3 \times 3}, I^{3 \times 3} \right], 0 \right)$ where: $B_1 = \nabla_{u(t)} F \big|_{P_1}$ and I stands for an identity matrix, the related transfer matrix $G_1(s)$ can be defined as:

$$G_1(s) \overset{\text{def}}{=} \frac{1}{D_1(s)} N_1(s), \tag{30}$$

_____

[1]To increase the legibility of the work the trajectories have been presented in extended domain, i.e., $(-2\pi, 2\pi]$.

(a) $(\theta_1, \dot{\theta}_1)$ – the first arm subspace
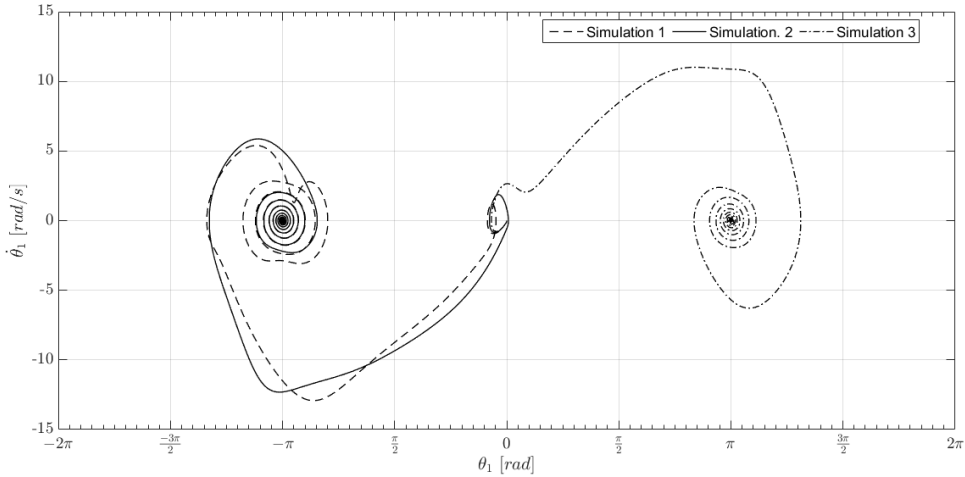
(b) $(\theta_2, \dot{\theta}_2)$ – the second arm subspace
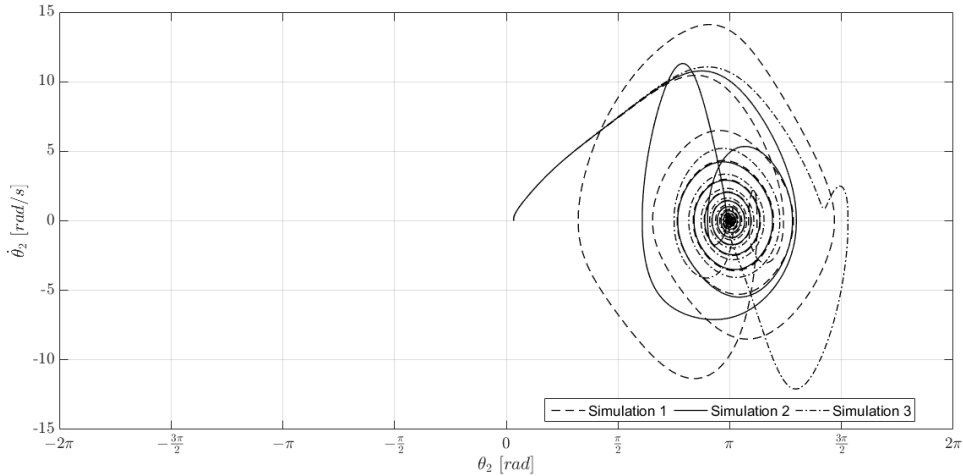
Figure 7: Phase portraits projection onto subspaces.

where: $D_1(s)$ is a transfer function denominator; $N_1(s)$ denotes a nominator of transfer matrix defined as:

$$\boldsymbol{N}_1(s) \stackrel{\text{def}}{=} \left[N_{1\,s}(s),\, N_{1\,\theta_1}(s),\, N_{1\,\theta_2}(s) \right]^T$$

which elements are directly related to the cart, first and second arm, respectively. Then the frequency properties of the DIP can be identified by $\boldsymbol{G}_1(s)|_{s=j\omega}$, where ω is the frequency.

For the set of arbitrary parameters (see Table 1 in Appendix A) roots of the particular numerators are as follows:

$$z\left(N_{1s}(s)\right) \approx [-16.80, \ -5.17, \ 6.15 + 0.12j, \ 6.15 - 0.12j], \quad (31a)$$
$$z\left(N_{1\theta_1}(s)\right) \approx [-11.78, \ 6.11, \ -0.35, \ 0.00], \quad (31b)$$
$$z\left(N_{1\theta_2}(s)\right) \approx [72.40, \ 12.11, \ -0.37, \ 0.00]. \quad (31c)$$

The above results show that for every subsystem of the DIP related to the cart, first and the second arm there are zeros of the transfer functions which are placed in the right half-plane of the complex plane. It implies that non-minimum phase behaviour around the upper position of the DIP is observed. This conclusion is also confirmed by Bode diagrams which have been presented in Fig. 8.

(a) Bode diagram of the DIP cart
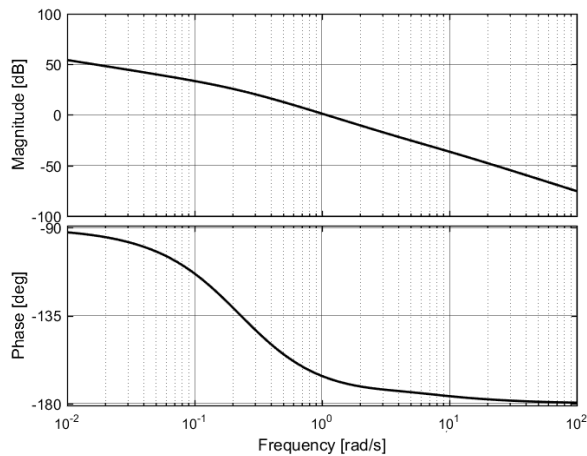
(b) Bode diagram of the DIP first arm
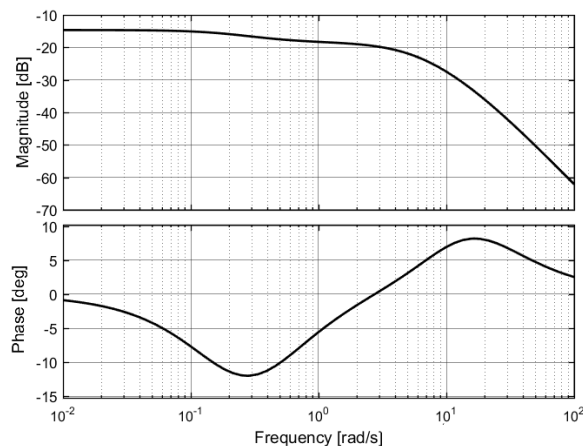
(c) Bode diagram of the DIP second arm

Figure 8: DIP Bode diagrams.

As it can be noticed in Fig. 8 there is no unique connection between corresponding magnitude and phase plots of the presented Bode diagrams.

5.   Conclusions

In this paper, the problem of mathematical modelling and indicating properties of the classical double inverted pendulum on the cart has been investigated. The derived DIP cognitive model is based on Euler-Lagrange formalism under several assumptions and in the presence of external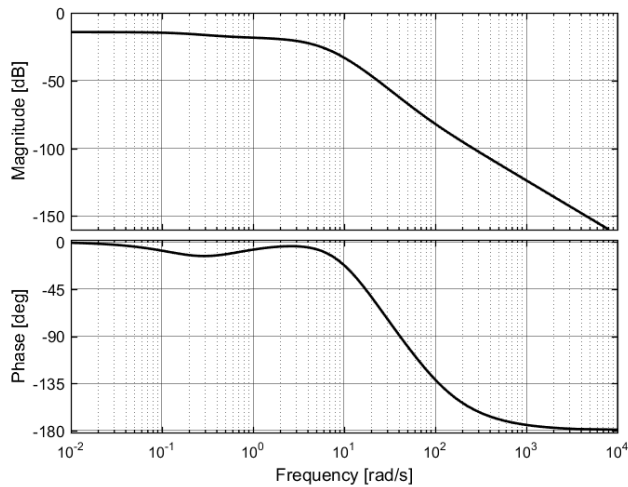 forces and friction. This model can be utilised for different purposes such as simulation, identification and control system synthesis. In turn, in order to confirm important properties of the DIP analytical as well as numerical tools have been used. The properties included stability of equilibrium points, a chaos of dynamics and non-minimum phase behaviour around an upper position. As the tools, the vector field, Lyapunov theory of stability, Lyapunov exponents, the phase portraits and Bode graphs have been employed. On the other hand, from the point of view of numerical implementation the transformation from DAE to ODE format has been derived. All presented considerations refer to the model of a physical (constructed) DIP system. Hence, in general, extensive knowledge about the DIP has been aggregated in the paper. It can be found interesting and useful for the relevant community, especially in engineering applications.

Appendix A

The values of the considered DIP parameters have been presented in Table 1. It is worth adding that these values correspond to the values of parameters of the real (constructed) pendulum, which have been measured or estimated during realisation of the BSc thesis [2].

Table 1: Parameters of the DIP.

No.	Parameter	Value	Unit
1.	m_0	$5301.68 \cdot 10^{-4}$	kg
2.	m_1	$183.69 \cdot 10^{-3}$	kg
3.	m_b	$1.09 \cdot 10^{-1}$	kg
4.	m_k	$0.28 \cdot 10^{-1}$	kg
5.	L_1	$231.38 \cdot 10^{-3}$	m
6.	L_2	$2.57 \cdot 10^{-1}$	m
7.	η_0	$0.10 \cdot 10^{0}$	kg m/s
8.	η_1	$0.01 \cdot 10^{0}$	kg m^2/s
9.	η_2	$0.01 \cdot 10^{0}$	kg m^2/s
10.	l_1	$145.27 \cdot 10^{-3}$	m
11.	l_2	$120.41 \cdot 10^{-3}$	m
12.	I_1	$165.56 \cdot 10^{-5}$	kg m^2
13.	I_b	$81.61 \cdot 10^{-5}$	kg m^2
14.	I_k	$0.43 \cdot 10^{-5}$	kg m^2
15.	m_2	$1379.52 \cdot 10^{-4}$	kg
16.	I_2	$135.18 \cdot 10^{-5}$	kg m^2
17.	u_{max}	$1.25 \cdot 10^{1}$	N

Appendix B

Principal symbols and abbreviations:

DAE   differential–algebraic equation,
DIP   double inverted pendulum,
ODE   ordinary differential equation,
$\mathcal{M}_{DIP}$ mathematical model of a physical DIP,

$\mathcal{M}_{\mathrm{DIP}}^{\mathrm{DAE}}$	$\mathcal{M}_{\mathrm{DIP}}$ in the DAE format,
$\mathcal{M}_{\mathrm{DIP}}^{\mathrm{ODE}}$	$\mathcal{M}_{\mathrm{DIP}}$ in the ODE format,
$\mathcal{M}_{\mathrm{DIP}}^{\mathrm{SS}}$	$\mathcal{M}_{\mathrm{DIP}}$ in the state space format,
$\dot{(\cdot)}$	derivative of $(\cdot)$ with respect to t,
$\ddot{(\cdot)}$	second derivative of $(\cdot)$ with respect to t,
$(\cdot)^T$	transposition operator identified for $(\cdot)$,
$(\cdot)^{-1}$	inverse operator identified for $(\cdot)$,
$\det(\cdot)$	determinant of $(\cdot)$,
$\nabla_{(\cdot)}$	gradient in the direction of $(\cdot)$,
$\times$	Cartesian product,
$\varnothing$	empty set,
η_0	friction coefficient between the cart and the gantry,
η_i	friction coefficient within ith joint, $\forall i \in \overline{1, 2}$,
λ_{L}	Lyapunov exponent,
$\xi_0(t)$	uncontrolled external force,
$\xi_i(t)$	ith uncontrolled external torque, $\forall i \in \overline{1, 2}$,
$\boldsymbol{\xi}(t)$	disturbance inputs vector,
$\theta_i(t)$	ith angular displacement, $\forall i \in \overline{1, 2}$,
$\mathbf{1}$	matrix with all elements equal 1,
D	Rayleigh dissipation function,
$D_1(s)$	transfer function denominator,
E_{k}	total kinetic energy,
E_{p}	total potential energy,
$\boldsymbol{G}_1(s)$	transfer matrix,
$\boldsymbol{I}$	identity matrix,
I_1	moment of inertia for the first arm,
I_2	equivalent moment of inertia including the second arm and the static load,
I_{b}	moment of inertia for the second arm,
I_{k}	moment of inertia for the the static load,
$\boldsymbol{F}$	general form of differential equation,
$F_{\mathrm{f}\,0}(t)$	viscous friction force between the cart and the gantry,
L	Lagrangian,
L_i	length of ith arm, $\forall i \in \overline{1, 2}$,
l_i	distance from the beginning of ith arm to its centre of gravity, $\forall i \in \overline{1, 2}$,
$M_{\mathrm{f}\,i}(t)$	viscous friction torque within ith joint, $\forall i \in \overline{1, 2}$,
m_0	mass of the cart,
m_1	mass of the first arm,
m_2	equivalent mass including the second arm and the static load,
m_{b}	mass of the second arm,

m_k	mass of the static load,
$N_1(s)$	nominator of transfer matrix,
P_j	jth equilibrium point, $\forall j \in \overline{1, 4}$,
$q(t)$	position vector,
Q	vector of external forces and torques,
$\mathbb{R}$	set of real numbers,
$s(t)$	linear displacement,
t	time instant,
$\mathbb{T}$	open set in $\mathbb{R}$,
$u(t)$	input force,
u_{max}	maximum input force,
$\mathbb{X}$	region in the state, control and disturbance input spaces combined,
$\mathbb{X}_d$	region in the disturbance input space,
$\mathbb{X}_q$	region in the state space,
$\mathbb{X}_u$	region in the control input space,
(X, Y, Z)	coordinate frame,
$\mathbb{Z}_+$	positive part of an integer field.

References

[1] I. Ali and M. Hossen: A two-wheeled self-balancing robot with dynamics model. In *Proceedings of the 4th International Conference on Advances in Electrical Engineering* (ICAEE), Dhaka, Bangladesh, 271–275, 2017.

[2] K. Andrzejewski, M. Czyżniewski, and M. Zielonka: *Synthesis and implementation of control system for double inverted pendulum*. BSc Thesis, Gdańsk University of Technology, (in Polish), 2017.

[3] R.P.M. Chan, K.A. Stol, and C.R. Halkyard: Review of modelling and control of two-wheeled robots. *Annual Reviews in Control*, **37**(1), (2013), 89–103.

[4] J. Chestnutt, M. Lau, G. Cheung, J. Kuffner, J. Hodgins, and T. Kanade: Footstep planning for the Honda ASIMO humanoid. In *Proceedings of the 2005 IEEE International Conference on Robotics and Automation*, Barcelona, Spain, 629–634, 2005.

[5] F. Dörfler and F. Bullo: Synchronization in complex networks of phase oscillators: A survey. *Automatica*, **50** (2014), 1539–1564.

[6] C. Gonzalez, I. Alvarado, and D. Muñoz La Peña: Low cost two-wheels self-balancing robot for control education. In *Proceedings of the 20th IFAC World Congress, Toulouse, France*, **50** (2017), 9174–9179.

[7] F. GRASSER, A. D'ARRIGO, S. COLOMBI, and A.C. RUFER: JOE: A mobile, inverted pendulum. *IEEE Transactions on Industrial Electronics*, **49**(1), (2002), 107–114.

[8] S. JADLOVSKÁ and J. SARNOVSKÝ: Classical double inverted pendulum - a complex overview of a system. In *Proceedings of the IEEE 10th Jubilee International Symposium on Applied Machine Intelligence and Informatics*, Herl'any, Slovakia, 103–108, 2012.

[9] J. KĘDZIERSKI and K. TCHOŃ: Feedback control of a balancing robot. In *Proceedings of the 14th IFAC Conference on Methods and Models in Automation and Robotics*, Miedzyzdroje, Poland, **42** (2009), 495–500.

[10] H.E. KHALIL: *Nonlinear systems*, 2nd edition. Prentice Hall, Upper Saddle River, New Jersey, US, 1996.

[11] Y. KIM, S H. KIM, and Y.K. KWAK: Dynamic analysis of a nonholonomic two-wheeled inverted pendulum robot. *Journal of Intelligent and Robotic Systems: Theory and Applications*, **44**(1), (2005), 25–46.

[12] U.E. KOCAMAZ, A. GÖKSU, H. TAŞKIN, and Y. UYAROĞLU: Synchronization of chaos in nonlinear finance system by means of sliding mode and passive control methods: A comparative study. *Information Technology and Control*, **44**(2), (2015), 172–181.

[13] I.D. LORAM and M. LAKIE: Human balancing of an inverted pendulum: position control by small, ballistic-like, throw and catch movements. *The Journal of Physiology*, **540** (2002), 1111—1124.

[14] M. MUHAMMAD, S. BUYAMIN, M.N. AHMAD, and S.W. NAWAWI: Dynamic modeling and analysis of a two-wheeled inverted pendulum robot. In *Proceedings of the 3rd International Conference on Computational Intelligence, Modelling and Simulation* (CIMSim), Langkawi, Malaysia, 159–164, 2011.

[15] H.G. NGUYEN, J. MORRELL, K.D. MULLENS, A.B. BURMEISTER, S. MILES, N. FARRINGTON, K.M. THOMAS, and D.W. GAGE: Segway robotic mobility platform. In D.W. Gage, editor, *Proceedings of SPIE Mobile Robots XVII*, vol. 5609, 207–220, 2004.

[16] M. PRASAD and N.W. NIRWAN: Design and fabrication of automatic balancing bicycle. *International Journal of Science, Engineering and Technology Research*, **5** (2016), 532–536.

[17] M. Rosenblum and A. Pikovsky: Synchronization: from pendulum clocks to chaotic lasers and chemical oscillators. *Contemporary Physics*, **44**(5), (2003), 401–416.

[18] Y. Sakagami, R. Watanabe, C. Aoyama, S. Matsunaga, N. Higaki, and K. Fujimura: The intelligent ASIMO: system overview and integration. In *Proceedings of the IEEE/RSJ International Conference on Intelligent Robots and Systems*, Lausanne, Switzerland, 2478–2483, 2002.

[19] B. Sawatzky, I. Denison, S. Langrish, S. Richardson, K. Hiller, and B. Slobogean: The segway personal transporter as an alternative mobility device for people with disabilities: A pilot study. *Archives of Physical Medicine and Rehabilitation*, **88** (2007), 1423–1428.

[20] J-J.E. Slotine and W. Li: *Applied nonlinear control*. Prentice Hall, Englewood Cliffs, New Jersey, US, 1991.

[21] N. Sozhamadevi and S. Sathiyamoorthy: Modeling and control of an unstable system using probabilistic fuzzy inference system. *Archives of Control Sciences*, **25**(3), (2015), 377–396.

[22] M.W. Spong: Underactuated mechanical systems. In B. Siciliano and K. P. Valavanis, editors, *Control Problems in Robotics and Automation. Lecture Notes in Control and Information Sciences*, vol. 230, Berlin, Heidelberg, 1998. Springer.

[23] T. Takei, R. Imamura, and S. Yuta: Baggage transportation and navigation by a wheeled inverted pendulum mobile robot. *IEEE Transactions on Industrial Electronics*, **56**(10), (2009), 3985–3994.

[24] M. Velazquez, D. Cruz, S. Garcia, and M. Bandala: Velocity and motion control of a self-balancing vehicle based on a cascade control strategy. *International Journal of Advanced Robotic Systems*, **13**(3), (2016), 1–11.

[25] S. Wenxia and C. Wei: Simulation and debugging of LQR control for two-wheeled self-balanced robot. In *Proceedings of the Chinese Automation Congress* (CAC), Jinan, China, 2391–2395, 2017.

[26] W. Zhong and H. Röck: Energy and passivity based control of the double inverted pendulum on a cart. In *Proceedings of the 2001 IEEE International Conference on Control Applications*, Mexico City, Mexico, 896–901, 2001.